

Reducing uncertainty in the AIRS radiometric calibration

Thomas S. Pagano^a, Evan M. Manning^a, Steven E. Broberg^a, Hartmut Aumann^a,
Margie Weiler^b, Larrabee Strow^c

^aJet Propulsion Laboratory, California Institute of Technology,
4800 Oak Grove Dr., Pasadena, CA 91109

^bBAE Systems, Nashua, New Hampshire, 03064 (Retired)

^cUniversity of Maryland Baltimore County (UMBC), Baltimore MD., 21250

ABSTRACT

The Atmospheric Infrared Sounder (AIRS) radiometric calibration coefficients convert the counts measured from the instruments A/D converters (Level 1A) to SI traceable radiance units (Level 1B). The calibration equations are based on how the instrument operates and follow a simple second order relationship between counts and radiance. Terms are included to account for nonlinearity of the detectors, emissivity and temperature knowledge of the on-board calibrator (OBC) blackbody and radiometric offset due to coupling of the polarization of the scan mirror with the spectrometer. In this paper, we re-derive the radiometric calibration equation with a little more rigor and account for the view angle of each of the 4 space views. We then derive new polarization coefficients from the 4 space views over the mission and use them to re-derive the coefficients for blackbody emissivity and nonlinearity. We then compare new coefficients (Version 7k) with the latest operational version of the AIRS radiometric calibration coefficients (Version 5). The AIRS Version 5 coefficients were sufficiently adequate that an update has never been made since AIRS launch in 2002. However, it can be seen, when we compare to the Cross-track Infrared Sounder (CrIS), that better agreement is made in Version 7. The impact of the new coefficients is highest at cold scene temperatures and very warm temperatures.

Keywords: AIRS, hyperspectral infrared, absolute, radiometric, calibration

1. INTRODUCTION

The Atmospheric Infrared Sounder (AIRS) is a hyperspectral infrared instrument on the EOS Aqua Spacecraft, launched on May 4, 2002. AIRS has 2378 infrared channels ranging from 3.7 μm to 15.4 μm and a 13.5 km footprint. The AIRS is a “facility” instrument developed by NASA as an experimental demonstration of advanced technology for remote sensing and the benefits of high resolution infrared spectra to science investigations¹. AIRS, in conjunction with the Advanced Microwave Sounding Unit (AMSU), produces temperature profiles with 1K/km vertical accuracy on a global scale, as well as water vapor profiles and trace gas amounts for CO₂, CO, SO₂, O₃ and CH₄. AIRS data are used for weather forecasting, climate process studies and validating climate models². For more information see <http://airs.jpl.nasa.gov>.

The AIRS instrument, developed by BAE SYSTEMS, incorporates numerous advances in infrared sensing technology to achieve a high level of measurement sensitivity, precision, and accuracy³. This includes a temperature-controlled spectrometer (157K) and long-wavelength cutoff HgCdTe infrared detectors cooled by an active-pulse-tube cryogenic cooler. It is this temperature control that is most likely responsible for the observed stability in the instrument. The Focal Plane Assembly (FPA) contains 12 modules with 15 individual PV HgCdTe line arrays of detectors in a 2 x N element arrays where N ranges from 94 to 192 for PV HgCdT, and 2 PC HgCdTe arrays with 1x 144, 130. Table 1 lists the modules. The AIRS acquires 2378 spectral samples at

Table 1. Module Spectral Regions

Array	Module	Wavelength	
		(min)	(max)
		(μm)	(μm)
1	M1a	3.7364	3.9169
2	M1b	4.11	4.3291
3	M2a	3.9149	4.11
4	M2b	4.3271	4.6085
5	M3	6.9356	7.4769
6	M4a	6.2003	6.4934
7	M4b	6.5504	6.85
8	M4c	7.4745	7.7921
9	M4d	7.8605	8.22
10	M5	8.8073	9.4796
11	M6	9.565	10.275
12	M7	10.275	10.985
13	M8	11.0704	11.7512
14	M9	11.7431	12.685
15	M10	12.7989	13.7457
16	M11	13.7377	14.5533
17	M12	14.6672	15.4

*Thomas.S.Pagano@jpl.nasa.gov, (818) 393-3917, airs.jpl.nasa.gov

resolutions, $\lambda/\Delta\lambda$, ranging from 1086 to 1570, in three bands: 3.75 μm to 4.61 μm , 6.20 μm to 8.22 μm , and 8.8 μm to 15.4 μm . AIRS scans the earth scene up to $\pm 49.5^\circ$ relative to nadir with a spatial resolution of 13.5 km. Each scan provides a full-aperture view of space and an on-board blackbody calibration source. The key to the high accuracy and NIST traceability of AIRS is the high quality On-Board Calibrator (OBC) blackbody, full aperture space view, and simple direct conversion of counts to radiances using a 2nd order polynomial with polarization correction. The OBC is a specular coated wedge design with an internal angle of 27.25° .

2. METHODOLOGY

2.1 Radiance Difference at the Detector

More information on the calibration design and an earlier version of the radiometric accuracy estimate can be found in the literature⁴. We derive the calibration coefficients from first principles again here for completeness and include a few more details.

In order to remove the instrument background and extract the Earth view radiance, we need to look at the difference between signals obtained while viewing Earth and those while viewing Space. We start with the assumption that the radiant power difference at the detector between the Earth view and space view referred to the aperture is a second order polynomial in the difference in counts. Written in this way, the coefficients represent the response of the instrument measured at the aperture.

$$P_{ev} - P_{sv} = RT[c_0 + c_1(dn_{ev} - dn_{sv}) + c_2(dn_{ev} - dn_{sv})^2] \quad (1)$$

P_{ev} = Power at the detector while viewing the Earth Scene for each footprint and scan (W)

P_{sv} = Power at the detector while viewing space for each scan (W)

RT = Product of the total AIRS reflection and transmission (unitless)

c_0 = Instrument offset (W/m²-sr- μm)

c_1 = Instrument gain (W/m²-sr- μm -counts)

c_2 = Instrument nonlinearity (W/m²-sr- μm -counts²)

dn_{ev} = Digital counts while viewing Earth for each footprint and scan (counts)

dn_{sv} = Digital counts while viewing Space for each scan (counts)

The signal measured by the AIRS detectors depends on the radiant power striking the detector plus the dark current. The signal can come from multiple sources including the scene and emission from the scan mirror and optics. We have shown that the radiance at the detector is also modulated by the coupling of the scan mirror polarization and the spectrometer polarization⁴.

$$P_{ev} = L_{ev}RT[1 + p_r p_t \cos 2(\theta - \delta)] + L_{sm}RT \left[\frac{\epsilon}{R} - p_r p_t \cos 2(\theta - \delta) \right] + P_{optics} \quad (2)$$

L_{ev} = Spectral Radiance in the Earth Viewport (W/m²-sr- μm)

L_{sm} = Spectral Radiance of the Scan Mirror for Unity Emissivity at T_{sm} (W/m²-sr- μm)

P_{optics} = Radiant Power at the detector from the optics (W)

ϵ = emission of the scan mirror (-)

$p_r p_t$ = Product of scan mirror and spectrometer polarization diattenuation (unitless)

θ = Scan Angle measured from nadir (radians)

δ = Phase of spectrometer polarization (radians)

The radiance at the detector while viewing space can be calculated from equation 2 by setting $L_{ev} = 0$. It includes the emission from the mirror and the optics and the polarization coupling term. For each space view mirror position, i , we have,

$$P_{sv,i} = L_{sm}RT \left[\frac{\epsilon}{R} - p_r p_t \cos 2(\theta_{sv,i} - \delta) \right] + P_{optics} \quad (3)$$

The power difference at the FPA is now

$$P_{ev} - P_{sv,i} = L_{ev}RT[1 + p_r p_t \cos 2(\theta - \delta)] +$$

$$\left\{ L_{sm}RT \left[\frac{\epsilon}{R} - p_r p_t \cos 2(\theta - \delta) \right] - L_{sm}RT \left[\frac{\epsilon}{R} - p_r p_t \cos 2(\theta_{sv,i} - \delta) \right] \right\} \quad (4)$$

or

$$P_{ev} - P_{sv,i} = L_{ev}RT[1 + p_r p_t \cos 2(\theta - \delta)] - L_{sm}RT p_r p_t [\cos 2(\theta - \delta) - \cos 2(\theta_{sv,i} - \delta)] \quad (5)$$

2.2 Calibration Equation

We can now include the instrument residual artifacts (polarization coupling) in the calibration equation. Substituting equation 6 into equation 1 and cancelling the RT we get

$$L_{ev}[1 + p_r p_t \cos 2(\theta - \delta)] - L_{sm} p_r p_t [\cos 2(\theta - \delta) + F_{sv}(\delta)] = \dots \\ c_0 + c_1(dn_{ev} - dn_{sv}) + c_2(dn_{ev} - dn_{sv})^2 \quad (6)$$

Solving for the Earth View Radiance, we get the calibration equation

$$L_{ev} = L_o(\theta) + \frac{c_0 + c_1(dn_{ev} - dn_{sv}) + c_2(dn_{ev} - dn_{sv})^2}{[1 + p_r p_t \cos 2(\theta - \delta)]} \quad (7)$$

Where the polarization offset is

$$L_o(\theta) = \frac{L_{sm} p_r p_t [\cos 2(\theta - \delta) - \cos 2(\theta_{sv,i} - \delta)]}{[1 + p_r p_t \cos 2(\theta - \delta)]} \quad (8)$$

$L_o(\theta) = \text{Polarized Mirror Emission Offset. (W/m}^2\text{-sr-}\mu\text{m)}$

2.3 Calibration Coefficients

The coefficients, c_i , of the instrument response are found pre-flight by fitting the observed radiances from a well calibrated external blackbody (substituted for L_{ev} in the calibration equation) to a second order polynomial in counts

$$[L_{ev} - L_o(\theta)][1 + p_r p_t \cos 2(\theta - \delta)] = c_0 + c_1(dn_{ev} - dn_{sv}) + c_2(dn_{ev} - dn_{sv})^2 \quad (9)$$

c_0 should be zero if L_o is calculated properly. Instability in this coefficient from test to test observed preflight, combined with its small magnitude has led us to set c_0 to zero leaving the full offset correction to the polarization term L_o . The linear coefficient c_1 obtained pre-flight is used to calibrate the OBC blackbody emissivity and temperature, but is updated on-orbit (see below). The nonlinear coefficient c_2 obtained pre-flight is used without modification in the calibration equation.

Then the radiometric calibration equation now be written as

$$L_{ev} = L_o(\theta) + \frac{c_0 + c_1'(dn_{ev} - dn_{sv}) + c_2(dn_{ev} - dn_{sv})^2}{[1 + p_r p_t \cos 2(\theta - \delta)]} \quad (10)$$

Where in-flight, the gain is then recalculated on-orbit for every scan using the OBC blackbody.

$$c_1' = \frac{\epsilon_{obc} P_{obc} [1 + p_r p_t \cos 2\delta] - L_o(180^\circ) - c_2(dn_{obc} - dn_{sv})^2 - c_0}{(dn_{obc} - dn_{sv})} \quad (11)$$

Where we have used $\theta_{OBC} = 180^\circ$ and $\cos 2(180^\circ - \delta) = \cos(2\delta)$. The effective emissivity is then

$$\epsilon_{obc} = \left\{ L_o(\theta_{obc}) + \frac{c_0 + c_1(dn_{obc} - dn_{sv}) + c_2(dn_{obc} - dn_{sv})^2}{[1 + p_r p_t \cos 2\delta]} \right\} / P_{obc} \quad (12)$$

where

$P_{obc} = \text{Plank Blackbody function of the OBC blackbody at temperature } T_{obc} \text{ (W/m}^2\text{-sr-}\mu\text{m)}$

$T_{obc} = \text{Telemetered temperature of the OBC blackbody (K) with correction of +0.3K.}$

$\epsilon_{obc} = \text{Effective Emissivity of the blackbody}$

$dn_{obc} = \text{Digital number signal from the AIRS while viewing the OBC Blackbody}$

We have included a +0.3K correction to the telemetered blackbody temperature. This correction was selected to account for biases calculated in the circuit diagram and I²R heating of the sensor⁵.

2.4 Space View Signal Bias Correction

In Version 5, the median of the 4 space views is taken without correction for the bias introduced by polarization and viewing angle. In this step we adjust each of the space views for the expected signal difference due to polarization relative to space view 1. Returning to equation 3, we can calculate the expected difference between space views $i=2, 3,$ and 4 and space view 1. Using $\cos 2(90^\circ - \delta) = -\cos 2\delta$.

$$(dn_{sv,i} - dn_{sv,1}) = -P_{sm}p_r p_t [\cos 2(\theta_{sv,i} - \delta) + \cos 2\delta] / c_1' \quad (13)$$

The difference can be subtracted from the $dn_{sv,i}$ of the space views to remove the mirror polarization bias and normalize them all to the angle of space view 1. If we approximate the position of space view 1 to be 90° (actual 91.7°) we can simplify the algebra and only impact the correction amount, already a small number, by $\sim 1\%$.

$$dn'_{sv,i} = dn_{sv,i} + P_{sm}p_r p_t [\cos 2(\theta_{sv,i} - \delta) + \cos 2\delta] / c_1' \quad (14)$$

We can now simplify the polarization offset term (equation 9) assuming all space views are at 90°

$$L_o(\theta) = \frac{L_{sm}p_r p_t [\cos 2(\theta - \delta) + \cos 2\delta]}{[1 + p_r p_t \cos 2(\theta - \delta)]} \quad (15)$$

In Version 7 we recommend the space view signal correction (equation 14) be applied to all space views 2, 3, and 4 prior to taking the mean or median of the 4. It is preferred to take the mean for channels with good noise performance.

2.5 Polarization Response from Space Views

We now present our derivation of the instrument polarization response terms $p_r p_t$ and δ . The AIRS views space at four different mirror positions every scan. Figure 1 shows the orientation of the scan and location of the space view and on-board calibrators. We can use this feature to extract the polarization response terms from the signals observed in the space view.

Starting with equation 7, and setting $L_{ev} = 0$, and substituting equation 8 we get

$$0 = \frac{L_{sm}p_r p_t [\cos 2(\theta - \delta) - \cos 2(\theta_{sv,i} - \delta)]}{[1 + p_r p_t \cos 2(\theta - \delta)]} + \frac{c_0 + c_1'(dn_{ev} - dn_{sv}) + c_2(dn_{ev} - dn_{sv})^2}{[1 + p_r p_t \cos 2(\theta - \delta)]} \quad (16)$$

Ignoring second order terms (the polarization signal is small so a nonlinear correction to the polarization is negligible) and setting c_0 to zero (assumes all offset differences between the Earth view and space views is due to mirror emission and polarization coupling).

$$(dn_{ev} - dn_{sv,i}) c_1' = -L_{sm}p_r p_t [\cos 2(\theta_{ev} - \delta) - \cos 2(\theta_{sv,i} - \delta)] \quad (17)$$

This relationship is true for all positions of the mirror, not just the earth view. Applying the equation for each of the space views relative to space view 1 and using the trig relationship,

$$\cos 2(\theta - \delta) = \cos 2\theta \cos 2\delta + \sin 2\theta \sin 2\delta \quad (18)$$

we can write the signal observed in the space view $i = 2, 3,$ or 4 relative to space view 1.

$$(dn_{sv,i} - dn_{sv,1}) c_1' = -L_{sm}p_r p_t [\cos 2\theta_{sv,i} \cos 2\delta + \sin 2\theta_{sv,i} \sin 2\delta + \cos 2\delta] \quad (19)$$

or

$$\frac{-(dn_{sv,i} - dn_{sv,1}) c_1'}{L_{sm}} = d_1 (1 + \cos 2\theta_{sv,i}) + d_2 \sin 2\theta_{sv,i} \quad (20)$$

where

$$d_1 = p_r p_t \cos 2\delta \quad (21)$$

$$d_2 = p_r p_t \sin 2\delta \quad (22)$$

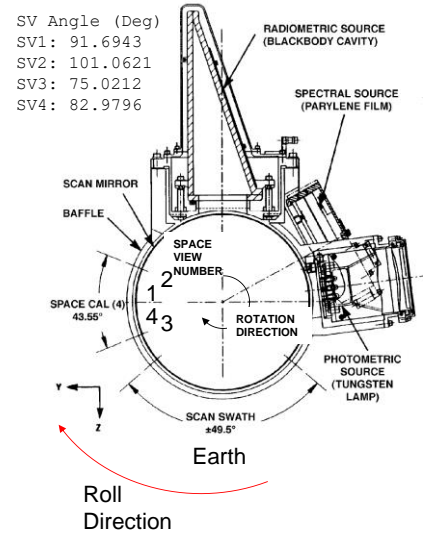


Figure 1. AIRS space views used to derive polarization parameters

We can fit the above equation using linear regression and solve for the coefficients

$$p_r p_t = \sqrt{d_1^2 + d_2^2} \quad (23)$$

The phase is calculated using equations 21 and 22 as

$$\delta = \frac{1}{2} \tan^{-1} \left(\frac{d_2}{d_1} \right) \quad (24)$$

The inverse tangent function constrains $-\pi/4 < \delta < \pi/4$ and can cause errors when the phase transitions from one sign to the opposite as the magnitude becomes greater than $\pi/4$. If the majority of values for δ within a module are positive, then values less than zero and greater than $|\delta_{\min}|$ are converted to $\delta = \delta + \pi/2$, and if the majority of values for δ within a module are negative, then values greater than zero and greater than $|\delta_{\min}|$ are converted to $\delta = \delta - \pi/2$. δ_{\min} varies by module to ensure values near zero are not changed in sign.

We must also determine the sign of the polarization amplitude term, $p_r p_t$, since the method in equation 23 computes only the amplitude. We first determine the polarization computed using the cosine function to determine the sign. That sign is then used to adjust the sign of the $p_r p_t$ derived from equation 23.

$$S_c = \frac{d_1}{\cos 2\delta} \quad (25)$$

$$p_r p_t' = p_r p_t \text{ sign}(S_c) \quad (26)$$

3. TEST DATA

3.1 In-Flight Space Views for Polarization Product and Phase

The process of determining the calibration coefficients for AIRS uses the above theory viewing well calibrated sources. We start with the space view data to derive the polarization related coefficients. The average counts for each of the 4 space views, $dn_{sv,i}$ for each day of the AIRS mission was collected and then averaged into values for each month. Data are filtered for bad space view 3 during certain parts of the orbit and averaged into 171 months from January 2003 through April 2017. The 4 space views for each month are used to compute the polarization product, $p_r p_t$, and phase, δ , from equations 20-24 for each month. A linear fit over all months is computed for each $p_r p_t$ and δ , and an offset and trend calculated. After calculation of the linear fit parameters for each channel, an 11 point running smooth is performed on all the channels within a module. The size of the window decreases near the edges of the module as fewer endpoints are available to smooth.

3.2 Pre-Flight Stepped Linearity Data for Residual Offset, OBC Blackbody Emissivity and Nonlinearity

The AIRS instrument is calibrated pre-flight by allowing the AIRS to view an external Large Area Blackbody (LABB) in the Earth view and a Space View Blackbody (SVBB) in the space view. In this test, called the ‘‘stepped LABB’’ test, the LABB is positioned either at nadir or 40 degrees and its temperature is raised from 205K to 310K and the digital counts from the instrument collected. We can use this data to calibrate the instrument radiometric response, and the OBC blackbody emissivity and temperature correction. The test data used are the same as in prior analyses⁶.

With the polarization parameters known, we can fit equation 9 to find the remaining radiometric coefficients, c_i , and the OBC blackbody emissivity and temperature correction. Data are obtained for A, B and AB gain settings for the LABB in the Earth viewport at nadir and 40 degrees. We only look at A or B data (not AB) due to the changing gain states over the mission. The LABB temperature is carefully controlled and used to derive L_{ev} , while signals from the instrument are obtained, dn_{LABB} for each test. The coefficients are derived by fitting a second order polynomial to the data for each channel for each of the 4 tests, A side nadir, B side nadir, A side 40 degrees, B side 40 degrees. All tests are averaged to derive the blackbody emissivity, but A side and B sides are treated separately as discussed below.

4. RESULTS

In this section we present the coefficients for the primary contributors to the radiometric calibration. We present the latest version, V7k, derived using the methodology above to coefficients derived preflight, V5 discussed in the literature⁴. The primary differences include a new methodology for computing mirror polarization using the 4 space views, increased smoothing of the blackbody emissivity coefficients and separate A side and B side nonlinearity coefficients. The end result produced a change in the radiometry that is not insignificant and agrees better with other data sets.

4.1 Polarization Product and Phase

Figure 2 shows the polarization product, $p_p p_t$, at $t=0$, or 2003, for the V7k data set compared to V5 (currently operational since launch). The general features are the same, but we see differences around 6 μm , and 14 μm , mostly due to the way the phase is calculated. In version 5, the phase term was zero, leaving the polarization term to do most of the work. We find higher residuals in the fit to the 4 space views if we force the phase term to be zero, indicating it should be non-zero. Figure 3 shows the drift in the polarization expressed as a percentage of the polarization itself. The polarization product term is very small, but we see as much as 10%/year change in some channels with most channels around 2%/year.

Figure 4 shows the phase, δ , at $t=0$, or 2003, for the V7k data set compared to V5 (zero phase). The V5 coefficients were determined preflight and there was not sufficient accuracy and sensitivity in the data to determine the phase so it was set to zero. Prior attempts to improve the polarization coefficients were hampered by the inability to achieve sufficient SNR to determine the phase⁷. The methods used, response vs scan angle pre-flight, and radiometric intercept, all had problems at cold scene temperatures. It is expected the LABB was not accurate at the coldest temperature of 200K, making the data unsuitable for polarization phase estimation. Figure 5 shows the drift in the phase expressed as a fraction of the impact to the correction. Although some values are high, the drift is usually less than 5% for most channels. The phase can be somewhat indeterminate as the polarization product goes to zero, so changes in phase may not be significant. The time dependence is carried for both phase and polarization product in the new version V7k.

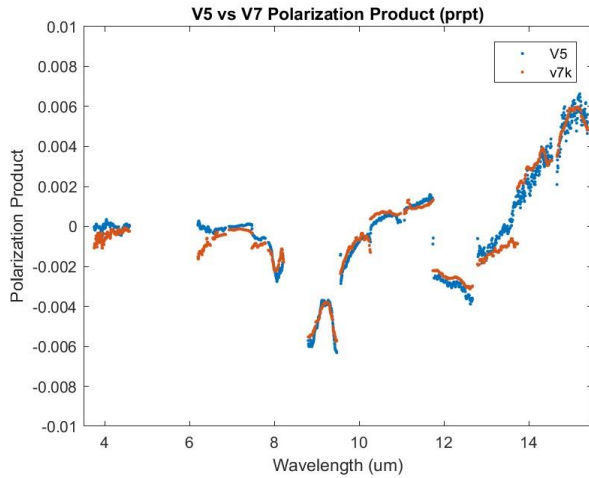


Figure 2. AIRS Polarization Product, $p_p p_t$

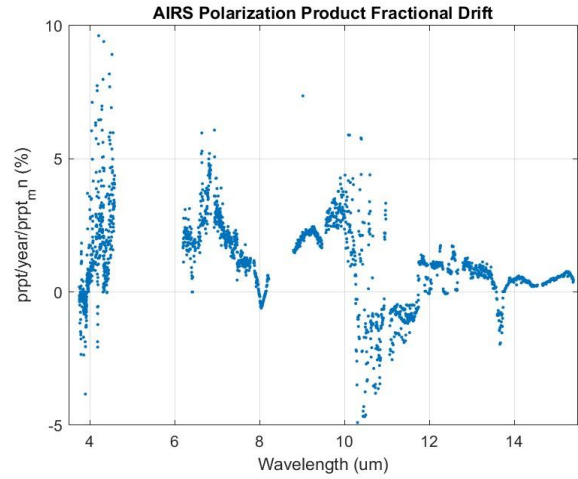


Figure 3. Annual drift in $p_p p_t$

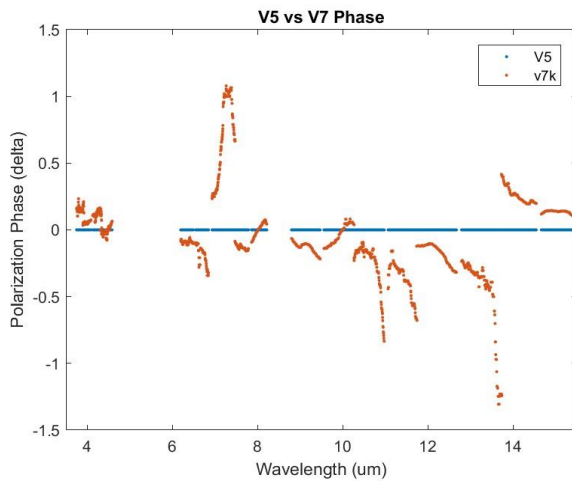


Figure 4. V7k has nonzero phase.

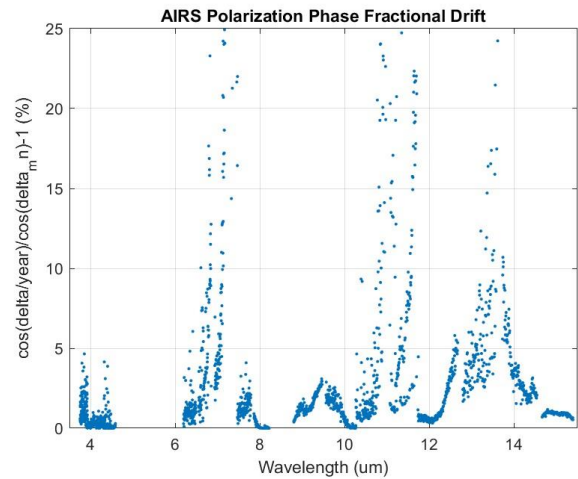


Figure 5. Annual drift in phase

4.2 OBC Blackbody Emissivity and Nonlinearity

Figure 6 shows the computed effective emissivity of the AIRS OBC obtained from equation 12 averaged over the 4 test obtained pre-flight. We saw some inconsistencies between the 4 data sets, yet there should be no difference amongst the test for this term. Since no other data sets are available, we compute the emissivity as the average of the four tests (A side, B side for Nadir and 40° incidence). We also perform a 501 channel smooth on the data to remove the artifact features at the boundary of modules most likely related to viewing geometry of the LABB in the near field. The resulting emissivity is compared to Version 5 in figure 6. We see the new emissivity is closer to unity in general.

Figure 7 shows the magnitude of the computed nonlinearity coefficient for Version 5 compared to Version 7k. In V7k, we carry separate A side and B side nonlinearity. Separate A side and B side calculations were made since we saw good consistency between sides at nadir and 40 degrees as expected since nonlinearity should also not be a function of scan position for a given side. We now compute separate coefficients for A and B sides as the mean for the nadir and 40 degree cases with the uncertainty as the standard deviation between the two tests. A 21 channel running smooth is applied to compute the mean 2nd order coefficient, c_2 .

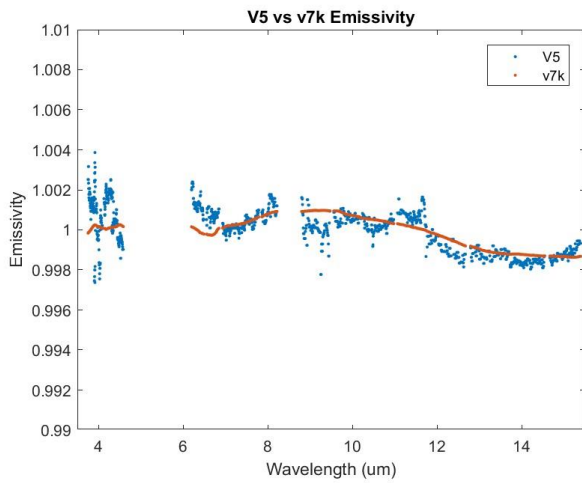


Figure 6. AIRS Effective emissivity

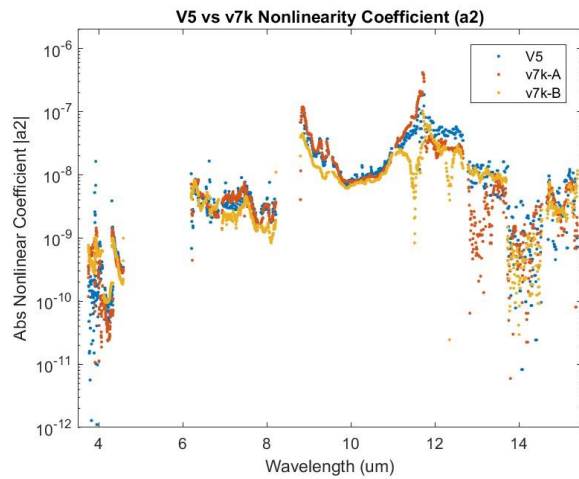


Figure 7. Magnitude of the AIRS Nonlinearity

4.3 Radiometric Differences between V5 and V7k

Figure 8 show the difference between Version 5 and Version 7k as a function of scene temperature. In this analysis the radiometric calibration equation was given a uniform scene temperature identified in the legend and coefficients for each of the two versions. The difference is calculated in radiance and divided by the radiance gradient at the scene temperature. The results show that at low scene temperatures as much as 1K difference is seen between the new and the old coefficients, while that difference is less than 0.2K at warm scene temperatures.

An important observation in Figure 8 is that the difference between the two versions has extremes near the module boundaries; particularly at cold scene temperatures. This is believed to be due to the improvement in the polarization and phase measurement. The AIRS polarization changes significantly near the module boundaries as seen in cross-axis scans of the polarization during preflight testing. In these tests, we see a distinct polarization dependence of the spatial response⁸.

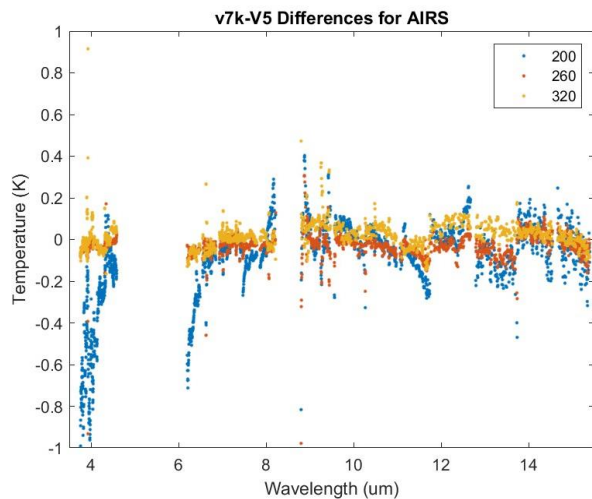


Figure 8. New V7k coefficients have biggest impact at low scene temperatures.

4.4 Comparison with CrIS

In this final section, we compare the radiometric differences between Version 7k and Version 5 to the differences seen between the Cross-track Infrared Sounder (CrIS) on the Suomi NPP satellite and AIRS. Both instruments have similar spectral ranges and spatial resolutions, however there are differences between the instrument Spectral Response Functions (SRFs) that must be accounted for. The process takes a large statistical sample of nadir data from AIRS and CrIS. Prior to comparing the AIRS to CrIS, we deconvolve the AIRS SRFs and reconvolve them to the CrIS SRFs. This requires the AIRS Level 1C which fills in gaps in the data due to failed or noisy channels. This process does result in some ringing in the spectrum so we perform a 7 point running smooth on the CrIS-AIRS data within a module prior to comparing. To compute the expected difference to be observed with V7k compared to V5, we use the average scene temperatures in the AIRS-CrIS comparisons for each channel (see Figure 9) in the radiometric calibration equation with each versions coefficients then take the radiometric difference. The temperature difference is the radiometric difference divided by the gradient of the Planck function with respect to temperature at the scene temperature.

The resulting temperature differences are plotted in Figure 10 for CrIS-AIRS and AIRS V7k-V5. The agreement looks good indicating that it is expected that if the CrIS-AIRS were redone with V7k, the differences would be much improved. We see discontinuities at module boundaries that might be mitigated, particularly around 13.8 microns and 9.5 microns. There appears to be a large difference at 6.8 microns between CrIS and AIRS that may not be improved in the new version that requires further investigation, but in general there appears to be evidence of an improvement. Results below 6 microns are not plotted in the figure due to sparser data points in the CrIS-AIRS, but the agreement is similar. In all cases there also appears to be a 100 mK warm bias between CrIS and AIRS (CrIS is warmer).

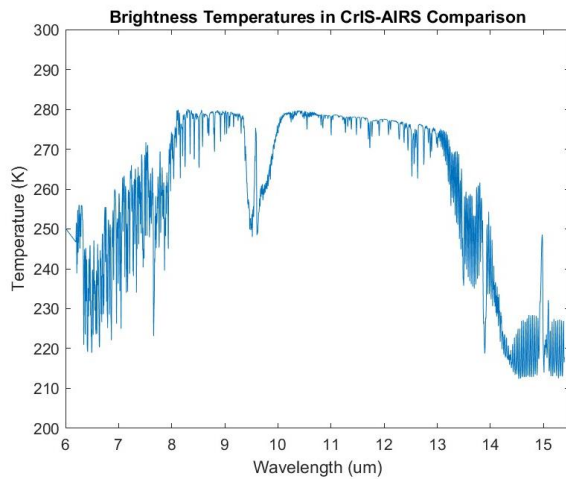


Figure 9. Average scene brightness temperature for random sample AIRS and CrIS scenes

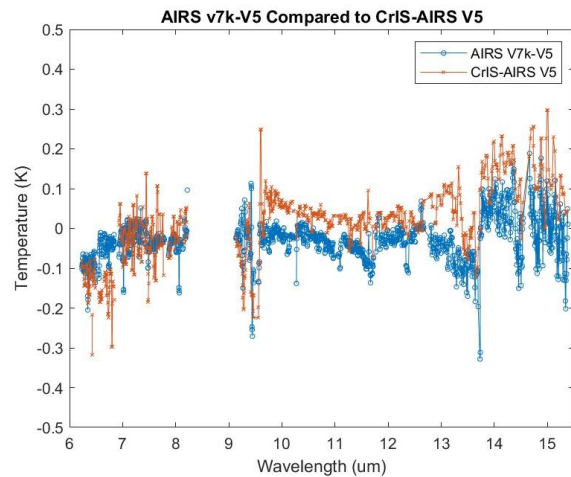


Figure 10. Average difference between CrIS and AIRS and difference between V7k and V5

SUMMARY AND CONCLUSIONS

Data acquired pre-flight and in orbit were used to determine the key coefficients for the AIRS radiometric calibration equation to convert counts obtained from the sensor to calibrated radiances. Inconsistencies in the offset term during the 4 tests obtained pre-flight led us to use in-flight data obtained from the 4 space views observed in-orbit to derive the polarization product and phase. The polarization data from in-flight have low noise and enable use of time dependent polarization and phase coefficients. Coefficients for OBC blackbody effective emissivity, temperature offset of the OBC and nonlinearity are derived from the pre-flight data sets since the data for these parameters are consistent over the multiple tests. The V7k coefficients now differ from V5 in that the polarization product and phase are time dependent variables and the nonlinearity has independent A side and B side coefficients. These two changes result in significant differences between V7k and V5, particularly at cold scene temperatures and shorter wavelengths. Uncertainties in the calibration are expected to be much lower in the new version but are not discussed in this paper. Comparisons between CrIS on the JPSS and AIRS show differences with much of the same behavior as the differences between V7k and V5 indicating that V7k should lead to an improvement in the agreement between the two instruments.

ACKNOWLEDGEMENTS

The research was carried out at the Jet Propulsion Laboratory, California Institute of Technology, under a contract with the National Aeronautics and Space Administration.

REFERENCES

- [1] Chahine, M.T., et al., "AIRS: Improving Weather Forecasting and Providing New Data on Greenhouse Gases", *Bulletin of the American Meteorological Society*, <https://doi.org/10.1175/BAMS-87-7-911>, (2006)
- [2] Pagano, T. S., M.T. Chahine, E.J. Fetzer, "The Atmospheric Infrared Sounder (AIRS) on the NASA Aqua Spacecraft: a general remote sensing tool for understanding atmospheric structure, dynamics and composition", *Proc. SPIE 7827-11*, (2010).
- [3] Morse, P., J. Bates, C. Miller, "Development and test of the Atmospheric Infrared Sounder (AIRS) for the NASA Earth Observing System (EOS)," *SPIE 3759-27*, July 1999.
- [4] Pagano, T. S.; Aumann, H.; Hagan, D. & Overoye, K. R., "Prelaunch and in-flight radiometric calibration of the Atmospheric Infrared Sounder (AIRS)", *IEEE T. Geoscience and Remote Sensing* 41 (2) , 265-273, (2003)
- [5] Pagano, T. S., H. Aumann, R. Schindler, D. Elliott, S. Broberg , K. Overoye, M. Weiler, "Absolute Radiometric Calibration Accuracy of the Atmospheric Infrared Sounder", *Proc SPIE*, 7081-46, San Diego, Ca, August 2008
- [6] Pagano, T.S., Aumann, H., Weiler, M., "Lessons learned from the AIRS pre-flight radiometric calibration", *Proc. SPIE 8866-30*, (2013).
- [7] Pagano, T. S., S. Broberg, M. Weiler, "Recent checks on the radiometric and spatial calibration of AIRS in-orbit", *Proc. SPIE 9972-7*, (2016)
- [8] Pagano, T. S., H. Aumann, L. Strow, "Pre-Launch Performance Characteristics of the Atmospheric Infrared Sounder", *SPIE 4169-41*, September 2000.

